Entropy production and stability during radial displacement of fluid in Hele–Shaw cell



2008 J. Phys.: Condens. Matter 20 465102

(http://iopscience.iop.org/0953-8984/20/46/465102)

IOP Publishing Journal of Physics: Condensed Matter

J. Phys.: Condens. Matter **20** (2008) 465102 (8pp) doi:10.1088/0953-8984/20/46/465102

# Entropy production and stability during radial displacement of fluid in Hele–Shaw cell

**L M Martyushev and A I Birzina**

Institute of Industrial Ecology, S. Kovalevskoi 20A, Ekaterinburg, 620219, Russia

E-mail: mlm@ecko.uran.ru

Received 30 May 2008, in final form 3 September 2008
Published 30 September 2008
Online at stacks.iop.org/JPhysCM/20/465102

**Abstract**

The entropy production in the problem of the radial displacement of a fluid in the Hele–Shaw cell is determined. The morphological stability of the interface between the displaced and displacing fluids is studied using the linear analysis for stability and the maximum entropy production principle. Regions, in which different forms of the interface can coexist, are predicted. These regions are analyzed depending on the cell size, the injected flow rate, and the ratio of the fluid viscosities.

## 1. Introduction

Investigators have long been interested [1–4] in the patterns that take shape as one less viscous fluid displaces the other in quasi-two-dimensional cells (Hele–Shaw cells), because of the diversity and beautiful appearance of the structures formed in simple experiments and the possible use of the results for solving environmental protection and petroleum production problems. From the theoretical standpoint this problem is also interesting since such problems can easily be reduced to sufficiently simple[1] and plausible mathematical models, which lend themselves to analytical analysis and demonstrate an interesting behavior. One of the issues receiving special emphasis is the study of the stability or instability of the interface between moving fluids. A perturbation (typically a harmonic one) is introduced by some means into a model and is analyzed. If the perturbation increases with time, the initial form is said to lose its stability. Usually this analysis can only be performed as a linear or a weakly nonlinear approximation [6–11]. Obviously, the interface stability to sufficiently small perturbations can only be judged from such calculations.

In recent decades an idea has emerged that the entropy production principle can be used to select from the different regimes of development of nonequilibrium evolving systems [12–14]. For example, the entropy production is calculated for competing processes and the process (the nonequilibrium phase) with the largest entropy production is assumed to be nonlinearly stable and, hence, observable with the highest probability. This rule follows from the maximum entropy production principle, which has been shown recently to be a fundamental principle in nonequilibrium thermodynamics and very fruitful in studies of dissipative systems [14–17]. A similar method of selection by means of entropy production was used earlier for analysis of morphological transitions during nonequilibrium crystallization [13, 18–22]. The analytical results obtained pointed to the possible coexistence of several nonequilibrium phases being in qualitative agreement with the relevant experimental observations. However, the quantitative comparison of the theoretical results (for example, the discovered regions of the coexistence) with the experimental data was practically impossible on account of the considerable simplifications introduced into the mathematical model of the phenomenon[2] and a very small (fractions of a micrometer) predicted size of the stability. Therefore it could not be stated with assurance that the method proposed earlier for the analysis of the stability of dissipative structures on the basis of the entropy production was valid. The problem of the displacement front stability in the Hele–Shaw cell is thought to be devoid of such shortcomings[3]. Therefore the objective of this study is the analytical analysis of the

[1] If compared with other hydrodynamic instabilities observed in experiments on Benard and Marangoni instability, laminar-turbulent transitions, etc.

[2] For the problem to possess an analytical solution, crystals were assumed to have a round or a spherical shape, the anisotropy was neglected, and so on.

[3] The mathematical model used for description of the displacement is much less crude and the experimentally observed critical sizes are much larger (of the order of centimeters).

 

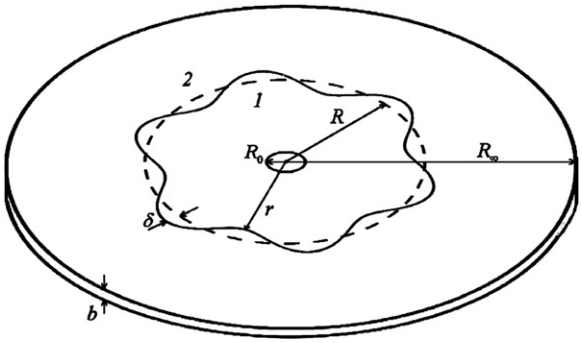


**Figure 1.** The radial displacement in the Hele–Shaw cell.

stability problem using the entropy production. The radial fluid displacement will be considered for definiteness. This study is the first analytical stage of the investigation. The experimental verification of the theoretical results will be published elsewhere.

It should be noted that calculations of the entropy production for analysis of the stability of the fluid front in the Hele–Shaw cell were used very little in previous studies. We are aware of two studies only. In the first study [23] it is concluded, from rather inexact reasoning, that the entropy production increases considerably as the displacement front of two immiscible fluids in a porous medium becomes unstable and fractal structures are formed. No other conclusions, except the quoted result, pertaining to the topic at hand were drawn. The author of the second paper [24] tried to analyze the stability of the radial displacement of two miscible incompressible fluids. The calculations and the results presented in this paper provoke some objections. Firstly, the expression for the entropy production disregards the contribution from the fluid mixing. Secondly, the work is extremely inconsistent: the entropy production is minimized at some calculation stages and is maximized at the others. Thirdly, the velocity field of the fluids was obtained in the linear order. This field was then used to calculate the relationship between the growth rate of the perturbation and its amplitude and, thus, the total excess energy dissipation rate (which was the basis of the calculation) proved to be quadratic relative to the amplitude.

## 2. Problem statement and the linear stability of the front

We shall consider a slow quasi-stationary displacement of a fluid by another fluid in the Hele–Shaw cell (figure 1). Both fluids are assumed to be immiscible and incompressible. The motion is quasi-two-dimensional and all characteristics of the flow are averaged over the cell thickness $b$. These approximations are traditional for problems of this type [1–11].

The pressure field in both fluids satisfies the Laplace equation:

$$\nabla^2 p_1 = 0, \tag{2.1}$$

$$\nabla^2 p_2 = 0. \tag{2.2}$$

This is the consequence of the Darcy law $\boldsymbol{V}_i = -M_i \nabla p_i$ ($M_i = b^2/12\mu_i$, $\mu_i$ being the fluid viscosity) and the flow continuity condition $\nabla \cdot \boldsymbol{V}_i = 0$. Here $p_i$ is the fluid pressure ($i$ = 1 and 2 for the displacing or the displaced fluid respectively) and $\boldsymbol{V}_i$ is the fluid velocity.

The pressures satisfy the following boundary conditions [6–10]:

$$-M_1 \partial p_1/\partial \boldsymbol{n}|_{R_0} = \frac{Q}{2\pi R_0}, \tag{2.3}$$

$$M_1 \partial p_1/\partial \boldsymbol{n}|_r = M_2 \partial p_2/\partial \boldsymbol{n}|_r, \tag{2.4}$$

$$p_1 - p_2|_r = \frac{2\varepsilon}{b} + \alpha V_n^\gamma + \beta K, \tag{2.5}$$

$$p_2|_{R_\infty} = 0, \tag{2.6}$$

where $\boldsymbol{n}$ is the normal to the surface, $V_n$ is normal velocity of the interface; $R_0$ is the radius of the hole through which the displacing fluid is injected at a constant flow rate ($Q$, cm$^2$ s$^{-1}$); $R_\infty$ is the size of the Hele–Shaw cell occupied by the displaced fluid; $r$ is the equation for the interface between two fluids; $\varepsilon$ is the surface tension; $K$ is the surface curvature in the motion plane; and $b$ is the cell thickness; $\alpha$, $\beta$ and $\gamma$ are some parameters (according to [2, 3, 10], $\alpha = 3.8\frac{2\varepsilon}{b}(\frac{\mu_2}{\varepsilon})^\gamma$, $\beta = \pi\varepsilon/4$ and $\gamma = 2/3$).

We shall assume that an arbitrarily small distortion of the initially round interface can be presented as a superposition of harmonic functions of the form $\cos(n\varphi)$. Considering the linear order approximation, it suffices to discuss the behavior of one function so as to understand the stability of the front. In the polar system of coordinates the equation for the perturbed surface is written in the form

$$r = R + \delta\cos(n\varphi), \tag{2.7}$$

where $R$ is the radius of the unperturbed surface; $\delta$ is the perturbation amplitude; $n$ is the perturbation frequency (see figure 1); and $\varphi$ is the polar angle.

The linear analysis for the stability [10] gives the following result:

$$p_i(r,\varphi) = p_i^0(r) + p_i^1(r,\varphi)\delta, \tag{2.8}$$

where

$$p_1^0 = -\frac{Q}{2\pi M_1}\ln(r/R) - \frac{Q}{2\pi M_2}\ln(R/R_\infty) + \frac{2\varepsilon}{b} + \frac{\beta}{R} + \alpha\left(\frac{Q}{2\pi R}\right)^\gamma, \tag{2.9}$$

$$p_2^0 = -\frac{Q}{2\pi M_2}\ln(r/R_\infty), \tag{2.10}$$

$$p_1^1 = a_1 r^n \cos(n\varphi)[1 + (R_0/r)^{2n}], \tag{2.11}$$

$$p_2^1 = a_2 r^n \cos(n\varphi)[1 - (R_\infty/r)^{2n}], \tag{2.12}$$

$$a_1 = R^{-n}\left[\frac{Q}{2\pi R}\frac{M_2 - M_1}{M_1 M_2} + \frac{\beta(n^2-1)}{R^2} - \frac{\alpha\gamma}{R}\left(\frac{Q}{2\pi R}\right)^\gamma\right] \times \left[\left[1 + (R_0/R)^{2n}\right] + \frac{M_1}{M_2}\frac{1 - (R/R_\infty)^{2n}}{1 + (R/R_\infty)^{2n}}\right.$$

$$\times \left[1-(R_0/R)^{2n}\right] + \alpha\gamma n\left(\frac{Q}{2\pi R}\right)^{\gamma}\frac{2\pi M_1}{Q}\left[1-(R_0/R)^{2n}\right]\Bigg]^{-1}, \quad (2.13)$$

$$a_2 = R^{-n}\left[\frac{Q}{2\pi R}\frac{M_2-M_1}{M_1M_2}+\frac{\beta(n^2-1)}{R^2}-\frac{\alpha\gamma}{R}\left(\frac{Q}{2\pi R}\right)^{\gamma}\right] \times \left[\frac{M_2}{M_1}\frac{1+(R_0/R)^{2n}}{1-(R_0/R)^{2n}}\left[1+(R_\infty/R)^{2n}\right] - \left[1-(R_\infty/R)^{2n}\right] + \alpha\gamma n\left(\frac{Q}{2\pi R}\right)^{\gamma}\frac{2\pi M_2}{Q}\left[1+(R_\infty/R)^{2n}\right]\right]^{-1}. \quad (2.14)$$

From (2.8) to (2.14) it is possible to find the critical size of the interface linear stability $R_S$ when the perturbation growth rate $\dot{\delta}$ reverses sign from negative (damping) to positive (growth). According to our earlier results [10], this size is determined from the equation

$$\dot{\delta}(R) = 0, \quad (2.15)$$

where

$$\dot{\delta} = \frac{\dot{R}}{R}\delta\Bigg\{-1-n\left(\frac{M_2}{M_1}-1\right) \times \left[1+\left((n^2-1)\frac{\beta}{R}-\alpha\,\gamma\left(\frac{Q}{2\pi R}\right)^{\gamma}\right)\frac{2\pi}{Q}\frac{M_1M_2}{M_2-M_1}\right] \times \left(\frac{M_2}{M_1}\frac{1+(R_0/R)^{2n}}{1-(R_0/R)^{2n}}+\frac{1-(R/R_\infty)^{2n}}{1+(R/R_\infty)^{2n}} + n\alpha\,\gamma\left(\frac{Q}{2\pi R}\right)^{\gamma}\frac{2\pi M_2}{Q}\right)^{-1}\Bigg\}, \quad (2.16)$$

$$\dot{R} = Q/2\pi R. \quad (2.17)$$

Obviously, the linear approximation allows the determination of the critical size of the stability $R_S$ when the interface of two fluids becomes unstable in the presence of perturbations having an infinitesimal amplitude. In terms of the classical theory of phase transitions this size may be called the spinodal of the nonequilibrium transition from the round shape to the finger (cosine-like) shape.

## 3. Entropy production during displacement of a fluid in the Hele–Shaw cell

### 3.1. General treatment

We shall consider the motion of a displaced homogeneous fluid in the Hele–Shaw cell. According to [25, 26], the density of the entropy production in a viscous isotropic incompressible fluid in a condition of isothermal vortex-free motion can be written in the form[4]

$$\sigma = -\overset{0}{\Pi}{}^{S} : (\overset{0}{\mathrm{Grad}}\, V)^{S}, \quad (3.1)$$

where $\overset{0}{\Pi}{}^{S}$ and $(\overset{0}{\mathrm{Grad}}\, V)^{S}$ are symmetrical parts of the stress and velocity gradient tensors, respectively, with a zero trace.

[4] The temperature is omitted from the denominator on the right of the expression (3.1) because under the isothermal conditions here it is of no significance for further discussion.

We shall assume that these tensors satisfy the classical linear relationship [25]

$$\overset{0}{\Pi}{}^{S} = -2\mu_2(\overset{0}{\mathrm{Grad}}\, V)^{S}. \quad (3.2)$$

Therefore the entropy production density can be written in the component form

$$\sigma = 2\mu_2\sum_{i,k}(\overset{0}{\mathrm{Grad}}\, V)^{S}_{ik}(\overset{0}{\mathrm{Grad}}\, V)^{S}_{ki}. \quad (3.3)$$

For the quasi-two-dimensional motion in the Hele–Shaw cell ($V_z = 0$) which is under consideration, the components of the tensor $(\overset{0}{\mathrm{Grad}}\, V)^{S}$ in cylindrical coordinates have the form [26]

$$(\overset{0}{\mathrm{Grad}}\, V)^{S} = \begin{pmatrix} \frac{\partial V_r}{\partial r} & \frac{1}{2}\left(\frac{\partial V_\varphi}{\partial r}-\frac{V_\varphi}{r}+\frac{1}{r}\frac{\partial V_r}{\partial \varphi}\right) & \frac{1}{2}\frac{\partial V_r}{\partial z} \\ \frac{1}{2}\left(\frac{\partial V_\varphi}{\partial r}-\frac{V_\varphi}{r}+\frac{1}{r}\frac{\partial V_r}{\partial \varphi}\right) & \frac{1}{r}\left(\frac{\partial V_\varphi}{\partial \varphi}+V_r\right) & \frac{1}{2}\frac{\partial V_\varphi}{\partial z} \\ \frac{1}{2}\frac{\partial V_r}{\partial z} & \frac{1}{2}\frac{\partial V_\varphi}{\partial z} & 0 \end{pmatrix}. \quad (3.4)$$

Therefore equation (3.3) may be rearranged to give

$$\sigma = 2\mu_2\Bigg\{\left(\frac{\partial V_r}{\partial r}\right)^2+\frac{1}{r^2}\left(\left(\frac{\partial V_\varphi}{\partial \varphi}\right)^2+2V_r\frac{\partial V_\varphi}{\partial \varphi}+V_r^2\right) + \frac{1}{2}\left[\frac{1}{r^2}\left(\frac{\partial V_r}{\partial \varphi}\right)^2+\frac{2}{r}\frac{\partial V_r}{\partial \varphi}\left(\frac{\partial V_\varphi}{\partial r}-\frac{V_\varphi}{r}\right)+\left(\frac{\partial V_\varphi}{\partial r}\right)^2 - \frac{2}{r}V_\varphi\frac{\partial V_\varphi}{\partial r}+\frac{1}{r^2}V_\varphi^2\right]\Bigg\}+\mu_2\left[\left(\frac{\partial V_r}{\partial z}\right)^2+\left(\frac{\partial V_\varphi}{\partial z}\right)^2\right]. \quad (3.5)$$

This expression can be divided into two parts: the first part corresponds to the energy dissipation in the plane $(r, \varphi)$, while the second part reflects the energy dissipation in the direction $z$, which is perpendicular to the fluid flow. Thus, in accordance with (3.5), the calculation of the entropy production requires that we know the three-dimensional field of the fluid velocity, but this knowledge is difficult to derive for many problems of hydrodynamics. However, the formula (3.5) can be considerably simplified for some hydrodynamic flows since many terms make a negligibly small contribution to the general dissipation. For example, referring to the problem formulated in section 2, we can write, in line with (2.8)–(2.12) and the Darcy law, for the displaced fluid:

$$V_r = -M_2\frac{\partial p_2}{\partial r} = \frac{Q}{2\pi r}-M_2\delta a_2 n\cos(n\varphi)(r^{n-1}+R_\infty^{2n}r^{-(n+1)}), \quad (3.6)$$

$$V_\varphi = -\frac{M_2}{r}\frac{\partial p_2}{\partial \varphi} = M_2\delta n a_2\sin(n\varphi)(r^{n-1}-R_\infty^{2n}r^{-(n+1)}). \quad (3.7)$$

Taking into account (3.6) and (3.7), the expression (3.5) can be considerably simplified by omitting the terms containing higher than the first order with respect to $\delta$:

$$\sigma \approx 2\mu_2\left\{\left(\frac{\partial V_r}{\partial r}\right)^2+\frac{1}{r^2}\left(2V_r\frac{\partial V_\varphi}{\partial \varphi}+V_r^2\right)\right\}+\mu_2\left(\frac{\partial V_r}{\partial z}\right)^2. \quad (3.8)$$

Considering the problem statement (section 2) the components of the flow velocity $(r, \varphi)$ across the Hele–Shaw cell are constant and are zero in the planes bounding the cell. To calculate the entropy production density of a small element of the volume having an area $r\,\mathrm{d}r\,\mathrm{d}\phi$ and thickness[5] $b$, we shall assume that the fluid velocity decreases from $V_r$ to zero in a narrow layer near the interface. In this case $V_r/b$ is the lower estimate of the last term in (3.8). If we are interested in the entropy production far from the hole through which the displacing fluid is injected ($r \gg R_0$), and since the thickness of the cell is small ($b < R_0$), then on account of (3.6) and (3.7) the first term in (3.8) can be neglected:

$$\sigma \approx \mu_2 \left(\frac{V_r}{b}\right)^2. \tag{3.9}$$

Thus, from (3.9) it is fairly simple to calculate[6] the entropy production for the displacement problem under consideration. This formula may prove to be insufficiently exact for determination of the absolute value of the entropy production. However, exact numerical values of $\sigma$ are of no interest in this study and, as we shall see in section 3.2, the above assumption does not lead to errors.

Equation (3.9) can be derived in a simpler way for the flow under consideration. The energy dissipation is due to the work done per unit time (the power) by viscous friction forces counteracting the fluid flow. Since we consider a stationary flow at a velocity $\boldsymbol{V}$, these forces are equal to the pressure gradient forces and, hence,

$$\sigma = -\boldsymbol{V} \cdot \nabla p \tag{3.10}$$

up to unessential constant factors.

Let us use the Darcy law and express the pressure gradient in terms of the velocity; then, using (3.6) and (3.7), write as a linear approximation:

$$\sigma \approx \frac{\mu_2}{b^2} V^2 \approx \mu_2 \left(\frac{V_r}{b}\right)^2.$$

The last expression exactly coincides with (3.9).

Let us make some comments on the application of (3.9) to the problem at hand.

(1) When one fluid is displaced by another fluid, the entropy is produced during motion of both fluids. The calculations for the displaced fluid (specifically, by equations (3.6) and (3.7)) are given in the foregoing. Obviously, a formula similar to (3.9) can also be deduced for the displacing fluid[7]. If the displacing fluid viscosity is assumed to be negligibly low, the energy dissipation by the motion of the displacing fluid may be neglected in the calculation of the total entropy production.

(2) A specific feature of the dissipation problem under consideration is the presence of both the interface between two moving fluids and the limiting surfaces of the Hele–Shaw cell (figure 1). The entropy production for one-phase flows [25, 26] far from interfaces is that discussed most frequently in the literature. The type of the problem considered herein is more specific, but has been considered as well [27, 28]. Notice that within the given problem statement the difficulties arising from the presence of two phases can be obviated for the following reasons. The limiting walls of the Hele–Shaw cell are assumed to be fully wetted with the displaced fluid, which forms a thin film as it moves. The fluids are thought to be absolutely immiscible and the interface is assumed to be infinitely thin. Therefore it is possible to disregard the entropy production contributed directly by the interface to the local entropy production in small finite elements of the volume even near the interface between the fluids. The effect of the interface on the energy dissipation of the moving fluids is due only to a distortion of the pressure field, leading to a change of motion velocity of the fluids on account of the boundary condition (2.5).

### *3.2. Variation of the entropy production upon transition from the stable to the unstable growth*

Let us treat the loss of the morphological stability from the standpoint of the nonequilibrium thermodynamics. Two displacement regimes are possible: first with a round interface between the displacing and displaced fluids and then, when some critical size is reached, with a cosine-like interface. The transition from one development regime to the other may be viewed as a nonequilibrium phase transition. In line with the maximum entropy production principle [16, 19] the most probable nonequilibrium phase will be the one with the maximum entropy production. Correspondingly the point at which the entropy productions of the two phases are equal is a specific point. Let us calculate this point[8]. According to (3.6) and (3.9), the entropy production density during the motion of a round interface equals

$$\sigma_0 \sim V_r^2 = \left(\frac{Q}{2\pi r}\right)^2 \tag{3.11}$$

up to constant factors.

For a cosine-like interface, in accordance with (3.6) and (3.9) the entropy production density in the linear order has the form

$$\sigma_p \sim \left(\frac{Q}{2\pi r}\right)^2 - \frac{Q}{\pi} M_2 \delta a_2 n \cos(n\varphi)(r^{n-2} + R_\infty^{2n} r^{-(n+2)}). \tag{3.12}$$

Let us compare the entropy productions for the perturbed $\Sigma_p$ and the unperturbed $\Sigma_0$ interface in a volume element of a unit thickness and an area limited by the angle $\mathrm{d}\varphi$. Since we are only interested in the initial moment of the loss of stability by the interface, the consideration will apply to the region near

[5] It is only this calculation of the entropy production averaged over the thickness of the cell that is possible for the problem formulated in section 2.

[6] To the lower estimate to be precise.

[7] It will differ from (3.9) by the viscosity and the velocity only.

[8] For definiteness we shall consider the entropy production during the motion of a more viscous displaced fluid.

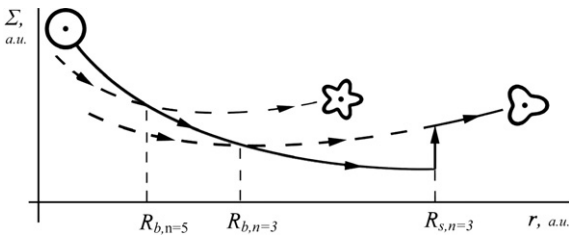


**Figure 2.** The entropy production near the interface of the fluids as a function of the interface spacing from the center of the Hele–Shaw cell. The solid line shows the behavior of the entropy production on the assumption that the displacement takes place in the absence of any perturbations. The abrupt change corresponds to the point of the absolute instability of the round interface as determined from the linear stability analysis. The dashed line shows the behavior of the entropy production for the perturbed interface. As soon as the binodal radius $R_b$ is reached, the entropy production for the perturbed interface becomes larger than that for the round interface.

the displacement front boundary:

$$\begin{aligned}\Sigma_p - \Sigma_0 &= \sigma_p r\,\mathrm{d}\varphi - \sigma_0 R\,\mathrm{d}\varphi \\ &= \sigma_p\,(R + \delta\cos(n\varphi))\,\mathrm{d}\varphi - \sigma_0 R\,\mathrm{d}\varphi \\ &\approx -\left[\left(\frac{Q}{2\pi R}\right)^2 + \frac{Q}{\pi} M_2 R^{n-1} a_2 n\left[1 + (R_\infty/R)^{2n}\right]\right] \\ &\quad\times \delta\cos(n\varphi)\,\mathrm{d}\varphi. \end{aligned} \tag{3.13}$$

Thus, the critical size, when the entropy productions are equal in the two displacement regimes, is found from the equation

$$\left(\frac{Q}{2\pi R}\right)^2 + \frac{Q}{\pi} M_2 R^{n-1} a_2 n\left[1 + (R_\infty/R)^{2n}\right] = 0. \tag{3.14}$$

This equation can only be solved numerically for $R$ and possesses a multitude of solutions. Obviously, only the solutions that fall within the interval from $R_0$ (the size of the inlet hole for the displacing fluid) to $R_S$ (the size when a round interface becomes absolutely unstable to infinitely small perturbations) are physically meaningful. The calculation shows that basically only one solution of (3.14)[9] fits this interval. This solution is labeled $R_b$. The numerical analysis of (3.13) and (3.14) shows that $\Sigma_0$ proves to be first larger and then, starting from the size $R_b$, smaller than $\Sigma_p$[10] (figure 2).

In line with the maximum entropy production principle and [16, 18–22], the size $R_b$ will be taken as the binodal of a nonequilibrium transition from one type of the displacement to the other, i.e. the size when the transition from the round to the cosine-like interface becomes theoretically possible in the presence of sufficient perturbations. Since at $R_S$ the transition under consideration becomes possible at an infinitely small perturbation, then, in accordance with [19–22], the region $[R_b, R_S]$ may be called a metastable (coexistence) region, i.e. the area where one or the other displacement regime (a nonequilibrium phase) can be observed depending on the perturbation amplitude. The behavior of this region depending on the control parameters of the problem will be analyzed in the next section. We shall close this section by making some comments.

(1) The value of $R_b$ was found by calculating the dissipation of the displaced fluid. It can be shown however that precisely the same result can be obtained from the dissipation of the displacing fluid.
(2) The literature often deals with a considerably simplified analytical statement of the problem concerning the displacement in the Hele–Shaw cell [6]. It is assumed that the cell is infinite ($R_\infty \to \infty$) and the hole, through which the fluid is displaced, is infinitely small ($R_0 \to 0$); the viscosity of the displacing fluid is neglected, $M_1 \to \infty$; and it is taken that $\alpha = 0$ and $\beta = \varepsilon$. In the given approximation the radii of the spinodal and the binodal are respectively equal to

$$\begin{aligned} R_{s,\mathrm{lim}} &= n(n+1)\frac{2\pi\varepsilon M_2}{Q}, \\ R_{b,\mathrm{lim}} &= \frac{n(n^2-1)}{(2n-1)}\frac{4\pi\varepsilon M_2}{Q}. \end{aligned} \tag{3.15}$$

It is difficult to use these formulae for quantitative comparison with relevant experimental data. But these approximations allow the analysis of the problem analytically rather than numerically.

## 4. Morphological diagrams

Let us perform the numerical analysis of the above results. Figures 3 and 4 present $R_S$ and $R_b$ as a function of the cell size and the flow rate for two displacements: the viscosity of the displacing fluid is much lower than, or is comparable, with the viscosity of the displaced fluid.

The results obtained suggest the following:

(1) The binodal and the spinodal exhibit similar behaviors. These radii become larger as the cell size increases and smaller as the displacement rate grows. A higher viscosity of the displacing fluid (figure 4) leads to an increase in the characteristic sizes of the stability loss. According to the calculations, the spinodal demonstrates the most specific behavior at perturbations with $n = 1$ (the translational instability): it is independent of the flow rate of the displacing fluid and has a linear dependence on the cell size. Notice that the dependence of the binodal on these parameters is rather weak at this perturbation.
(2) The binodal is always smaller than the spinodal for one and the same harmonic. However, spinodals and binodals relating to different disturbing harmonics can mutually intersect. The higher the viscosity of the displacing fluid, the larger the number of these intersections. This can be better appreciated from figure 5. The calculation results show that as the viscosity ratio increases, the stability radii first change rather insignificantly, but then start increasing sharply. The lower the disturbing harmonic, the earlier the increase begins and, consequently, $R_S$ and $R_b$ of adjacent harmonics start intersecting. The larger the $\mu_1/\mu_2$ ratio, the greater the number of intersections and, hence, the

[9] An exception will be noted further in the text.
[10] The sign alteration is estimated for the convex part of the interface.

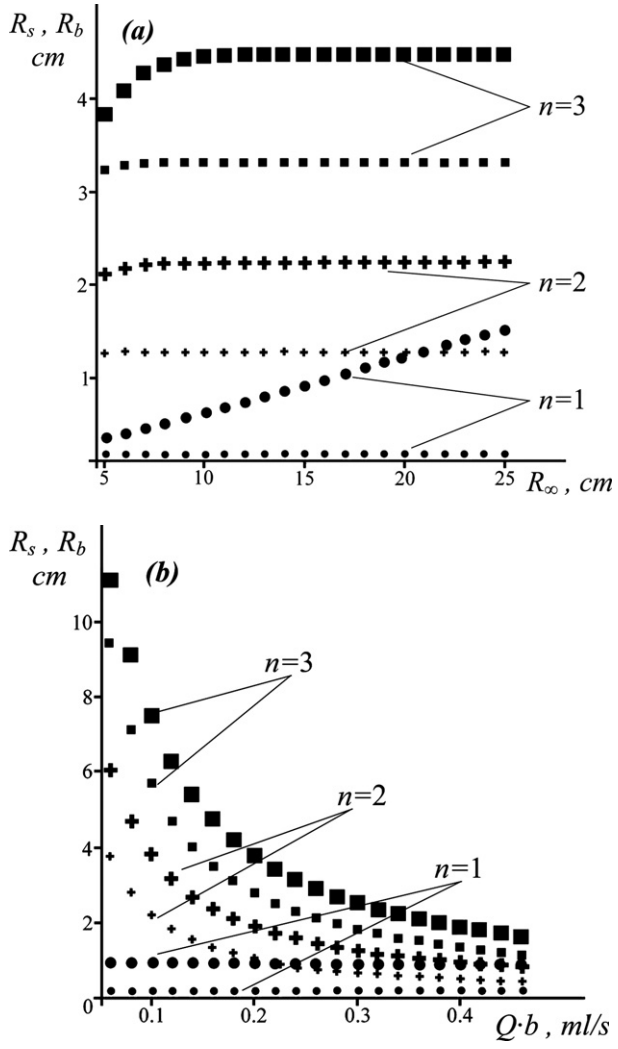


**Figure 3.** Dependence of the spinodal radius $R_S$ and the binodal radius $R_b$ (a) on the cell size $R_\infty$ at a constant volume flow rate $Q \cdot b = 0.17$ ml s$^{-1}$ and (b) on the volume flow rate $Q \cdot b$ at a constant cell size $R_\infty = 15$ cm. The curves were plotted taking $R_0 = 2$ mm, $b = 0.6$ mm, $\varepsilon = 33 \times 10^{-3}$ N m$^{-1}$, $\mu_1 = 1.72 \times 10^{-5}$ kg m$^{-1}$ s$^{-1}$ and $\mu_2 = 4.65 \times 10^{-3}$ kg m$^{-1}$ s$^{-1}$ (the viscosity and the surface tension correspond to those of air and silicon oil (PMS-5 in Russian classification)). The spinodal and binodal radii are marked with large and small symbols, respectively.

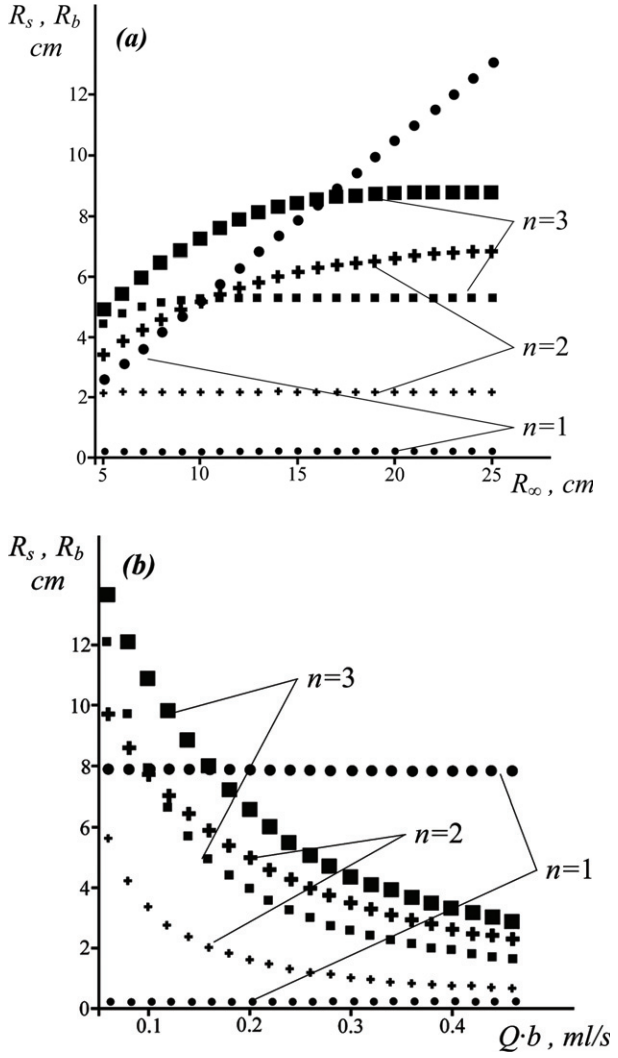


**Figure 4.** The dependence of the spinodal radius $R_S$ and the binodal radius $R_b$ (a) on the cell size $R_\infty$ at a constant volume flow rate $Q \cdot b = 0.15$ ml s$^{-1}$ and (b) on the volume flow rate $Q \cdot b$ at a constant cell size $R_\infty = 15$ cm. The curves were plotted taking the same parameters as in figure 3, except $\mu_1 = 1 \times 10^{-3}$ kg m$^{-1}$ s$^{-1}$ (the water viscosity). The spinodal and binodal radii are marked with large and small symbols, respectively.

more diverse and complicated is the sequence of the morphological transitions from the round to the cosine-like interfaces. Some examples are given in figure 6. Let us explain a few of them. At small $\mu_1/\mu_2$ ($\mu_1/\mu_2 = 0.0003$) the sequence of nonequilibrium phases is the simplest: the initially round interface becomes translation-unstable at the perturbation with $n = 1$ starting from some size $R_b$ and then absolutely unstable to this type of perturbation when the size equals $R_S$. If $\mu_1/\mu_2 = 0.05$, the metastable region widens and the number of possible nonequilibrium phases, which can coexist in this region depending on perturbations, rises to three ($n = 0, 1, 2$). They appear in sequence: a round interface ($n = 0$) is observed first, then the phase with $n = 1$ and, finally, the phase with $n = 2$ can appear starting from some size. If the phase with $n = 0$ does not transform to the phases with $n = 1$ and 2 during its metastable growth[11], it will turn into a nonequilibrium phase with $n = 2$ because in accordance with the calculation the spinodal radius at $n = 2$ is the smallest. At $\mu_1/\mu_2 = 0.2$ and $\mu_1/\mu_2 = 0.3$ the development is still more diverse (five and six morphological phases can coexist in the metastable region respectively). The last example with $\mu_1/\mu_2 = 0.58$ is interesting. It shows that the formation sequence of possible phases in the metastable region does not always coincide with $n$. In the given case, nonequilibrium phases with $n = 3$ and then with 4, 2 and 5 can appear first, while the phase with $n = 1$ will be the last.

It is seen from figure 6 that as $\mu_1/\mu_2$ increases, the smallest spinodal radius changes successively: from $R_S$ for

[11] Sufficient perturbations do not occur during development of the phase.

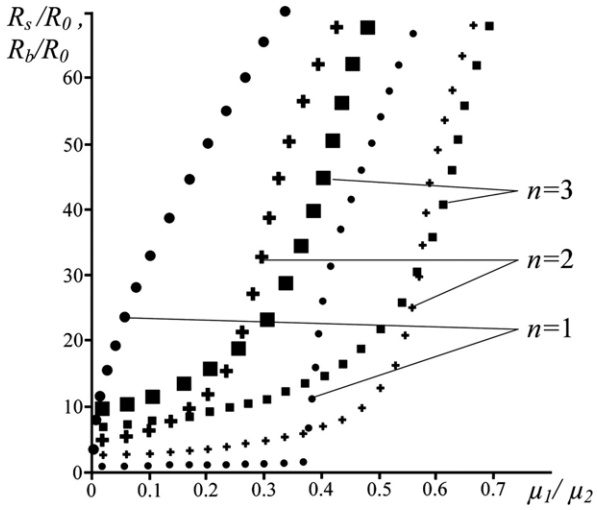


**Figure 5.** The dependence of $R_S/R_0$ and $R_b/R_0$ on $\mu_1/\mu_2$. The curves were plotted taking $Q \cdot b = 0.4$ ml s$^{-1}$, $R_\infty = 20$ cm, $R_0 = 2$ mm, $b = 0.6$ mm, $\varepsilon = 33 \times 10^{-3}$ N m$^{-1}$ and $\mu_2 = 4.65 \times 10^{-3}$ kg m$^{-1}$ s$^{-1}$. The spinodal and binodal radii are marked with large and small symbols, respectively.

$n = 1$ to $R_S$ for $n = 4$. However, the calculation showed that at large viscosity ratios neighboring spinodal radii can exchange places more than once. For example, if $Q \cdot b = 0.7$ ml s$^{-1}$ (the other parameters are similar to those used in figure 5), then the spinodal for $n = 4$ is observed as $\mu_1/\mu_2$ changes from 0.4 to 0.52 and the spinodal for $n = 5$ is observed as $\mu_1/\mu_2$ changes from 0.52 to 0.56; the spinodal for $n = 4$ again becomes the first (the smallest) starting from $\mu_1/\mu_2 = 0.56$. The value of $R_b$ exhibits an analogous behavior.

Generally, out of the many solutions to the equation (3.14), only one root fits the interval from $R_0$ to $R_S$, while the other solutions are beyond this interval and, hence, are devoid of any physical meaning. However, the numerical analysis suggests that at $n = 1$ there is some region of values of the viscosity ratio and the fluid flow rate where more than one root of the equation (3.14) can fall within the interval $[R_0, R_S]$. For example, at $\mu_1/\mu_2 = 0.39$, $Q = 0.3$ ml s$^{-1}$, $b = 0.6$ mm, $R_0 = 0.2$ cm and $R_S = 15.9$ cm the equation (3.14) possesses three solutions $R_b = 0.4, 2.2, 3.4$ cm. In line with the maximum entropy production principle and [16, 18–22] we can interpret this result in the following way. The phase with $n = 1$ appears if $\Sigma_p > \Sigma_0$ during the displacement process and cannot appear[12] if $\Sigma_p < \Sigma_0$.

## 5. Conclusion

Thus, possible sequences of morphological transitions during the displacement of a fluid in the Hele–Shaw cell are predicted on the basis of the maximum entropy production principle. The obtained results demonstrate a considerable diversity of possible morphological phase diagrams. A significant point is that the calculations can rather easily be verified in experiments, since the regions, in which a particular shape of the interface can be observed (singly or jointly with the others) or be absent (unstable), are clearly defined. The old theory [6–10, 24] does not provide such advantages. So, the linear stability analysis allows the determination of just one boundary, namely the stability to infinitesimal perturbations. It was not stated what the transition will be (sub-or supercritical) if the perturbation is not infinitely small. Therefore the result of any experiment could not contradict the theoretical prediction since any discrepancy could always be explained as the perturbations in any real experiment not being infinitesimal. This experimental unfalsifiability is a considerable drawback of the linear analysis[13]. The approach described herein is more favorable in this respect because the experimental validation of theoretical results is possible and this validation will be described in our future papers.

[12] In this case only the unperturbed phase exists.

[13] A similar reasoning applies to the weakly nonlinear stability analysis [11].

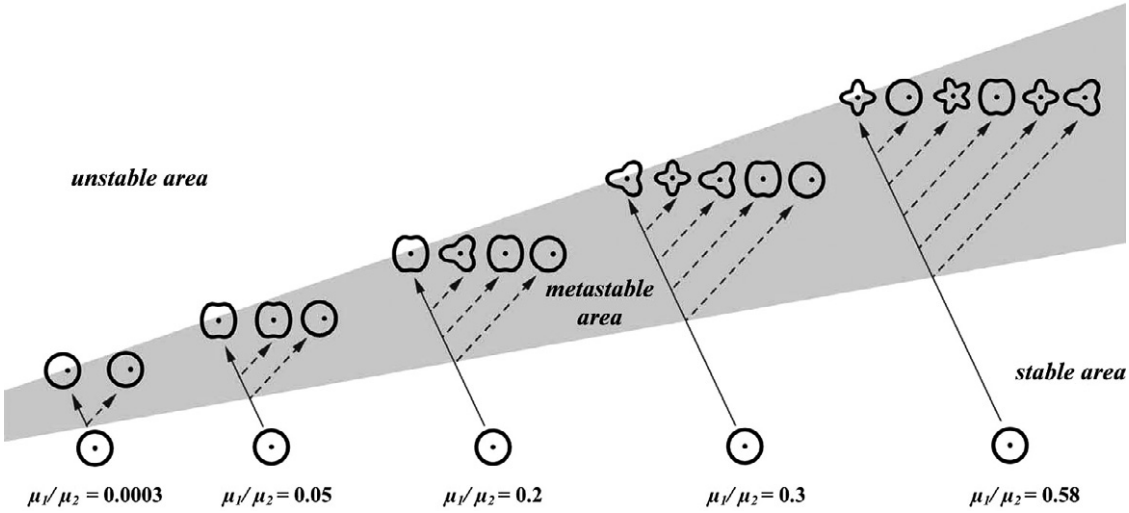


**Figure 6.** The possible sequence of structures during the displacement in the Hele–Shaw cell at different viscosity ratios $\mu_1/\mu_2$. The parameters are similar to those used in figure 5.

## Acknowledgments

The authors wish to thank Professor V D Seleznev for the discussion of basic ideas in this study and D A Gorchakov for his help in preparing the manuscript. This work was partially supported by the Russian Foundation for Basic Research (grant no. 070800-139).

## References

[1] Saffman P G and Taylor G 1958 The penetration of a fluid into a porous medium or Hele–Shaw cell containing a more viscous liquid *Proc. R. Soc.* A **245** 312–29
[2] Bensimon D, Kadanoff L P, Liang S, Shraiman B I and Chao T 1986 Viscous flows in two dimensions *Rev. Mod. Phys.* **58** 977–99
[3] Homsy G M 1987 Viscous fingering in porous media *Annu. Rev. Fluid Mech.* **19** 271–311
[4] Kessler D A, Koplik J and Levin H 1988 Pattern selection in fingered growth phenomena *Adv. Phys.* **37** 255–339
[5] McCloud K V and Maher J V 1995 Experimental perturbations to Saffman–Taylor flow *Phys. Rep.* **260** 139–85
[6] Paterson L 1981 Radial fingering in a Hele–Shaw cell *J. Fluid Mech.* **113** 513–29
[7] Ben-Jacob E *et al* 1986 Formation of a dense branching morphology in interfacial growth *Phys. Rev. Lett.* **57** 1903–6
[8] Buka A and Palffy-Muhoray P 1987 Stability of viscous fingering patterns in liquid crystals *Phys. Rev.* A **36** 1527–9
[9] Martyushev L M and Birzina A I 2008 Morphological stability of the interphase boundary of a fluid displaced in a finite Hele–Shaw cell *Tech. Phys. Lett.* **34** 213–6
[10] Martyushev L M and Birzina A I 2008 Specific features of the loss of stability during radial displacement of fluid in the Hele–Shaw cell *J. Phys.: Condens. Matter* **20** 045201
[11] Miranda J A and Widom M 1998 Radial fingering in a Hele–Shaw cell: a weakly nonlinear analysis *Physica* D **120** 315–28
[12] Shimizu H and Sawada Y 1983 Relative stability among metastable steady state structures in chemical reaction systems *J. Chem. Phys.* **79** 3828–35
[13] Ben-Jacob E and Garik P 1990 The formation of pattern in non-equilibrium growth *Nature* **343** 523–30
[14] Ozawa H, Ohmura A, Lorenz R D and Pujol T 2003 The second law of thermodynamics and the global climate system: a review of the maximum entropy production principle *Rev. Geophys.* **41** 1018
[15] Ziegler H 1983 *An Introduction to Thermomechanics* (Amsterdam: North-Holland)
[16] Martyushev L M and Seleznev V D 2006 Maximum entropy production principle in physics, chemistry and biology *Phys. Rep.* **426** 1–45
[17] Kleidon A and Lorenz R D (ed) 2004 *Non-Equilibrium Thermodynamics and the Production of Entropy in Life, Earth, and Beyond* (Berlin: Springer)
[18] Hill A 1990 Entropy production as the selection rule between different growth morphologies *Nature* **348** 426–8
[19] Martyushev L M, Seleznev V D and Kuznetsova I E 2000 Application of the principle of maximum entropy production to the analysis of the morphological stability of a growing crystal *JETP* **91** 132–43
[20] Martyushev L M, Kuznetsova I E and Seleznev V D 2002 Calculations of the complete morphological phase diagram for nonequilibrium growth of a spherical crystal under arbitrary surface kinetics *JETP* **94** 307–14
[21] Martyushev L M and Sal'nicova E M 2003 Morphological transition in the development of a cylindrical crystal *J. Phys.: Condens. Matter* **15** 1137–46
[22] Martyushev L M 2007 Some interesting consequences of the maximum entropy production principle *JETP* **104** 651–4
[23] Ametov I M 1999 Entropy analysis of a fluid filtration *J. Eng. Phys. Thermophys.* **72** 24–30
[24] Paterson L 1985 Fingering with miscible fluid in a Hele–Shaw cell *Phys. Fluids* **28** 26–30
[25] De Groot S R and Mazur P 1962 *Non-Equilibrium Thermodynamics* (Amsterdam: North-Holland)
[26] Landau L D and Lifshitz E M 1959 *Fluid Mechanics* (Oxford: Pergamon)
[27] Bedeaux D, Albano A M and Mazur P 1976 Boundary conditions and non-equilibrium thermodynamics *Physica* A **82** 438–62
[28] Caroly B, Caroly C and Roulet B 1984 Non-equilibrium thermodynamics of the solidification problem *J. Cryst. Growth* **66** 575–85